



# Transcranial direct current stimulation modulates brain functional connectivity in autism

Tianyi Zhou<sup>a</sup>, Jiannan Kang<sup>b</sup>, Zheng Li<sup>a</sup>, He Chen<sup>c</sup>, Xiaoli Li<sup>c,\*</sup>

<sup>a</sup> Center for Cognition and Neuroergonomics, State Key Laboratory of Cognitive Neuroscience and Learning, Beijing Normal University, Zhuhai 519087, China

<sup>b</sup> College of Electronic & Information Engineering, Hebei University, Baoding, China

<sup>c</sup> State Key Laboratory of Cognitive Neuroscience and Learning, IDG/McGovern Institute for Brain Research, Beijing Normal University, Beijing 100875, China

## ARTICLE INFO

### Keywords:

Autism spectrum disorder  
Transcranial direct current stimulation  
Network-based approaches  
Brain plasticity  
Frequency-dependent subnetworks

## ABSTRACT

Autism spectrum disorder (ASD) is characterized by deficits in social interactions, impairments in language and communication, and highly restricted behavioral interests. Transcranial direct current stimulation (tDCS) is a widely used form of noninvasive stimulation and may have therapeutic potential for ASD. So far, despite the widespread use of this technique in the neuroscience field, its effects on network-level neural activity and the underlying mechanisms of any effects are still unclear. In the present study, we used electroencephalography (EEG) to investigate tDCS induced brain network changes in children with ASD before and after active and sham stimulation. We recorded 5 min of resting state EEG before and after a single session of tDCS (of approximately 20 min) over dorsolateral prefrontal cortex (DLPFC). Two network-based methods were applied to investigate tDCS modulation on brain networks: 1) temporal network dynamics were analyzed by comparing “flexibility” changes before vs after stimulation, and 2) frequency specific network changes were identified using non-negative matrix factorization (NMF). We found 1) an increase in network flexibility following tDCS (rapid network configuration of dynamic network communities), 2) specific increase in interhemispheric connectivity within the alpha frequency band following tDCS. Together, these results demonstrate that tDCS could help modify both local and global brain network dynamics, and highlight stimulation-induced differences in the manifestation of network reconfiguration. Meanwhile, frequency-specific subnetworks, as a way to index local and global information processing, highlight the core modulatory effects of tDCS on the modular architecture of the functional connectivity patterns within higher frequency bands.

## 1. Introduction

In the last two decades, transcranial direct current stimulation (tDCS) has made remarkable contributions to neuroscience (Dedoncker et al., 2016). Non-invasive brain stimulation techniques are assumed to directly modulate neuronal activity by means of sustaining weak direct currents (Kunze et al., 2016; Mancini et al., 2016). Recently, abundant evidence has supported the capability of such currents to induce polarity-specific effects that are not strictly restricted to the stimulated site (Mancini et al., 2016; Keeser, 2011; Pellicciari et al., 2013). Since electrical stimulation affects large areas of cortex, tDCS-induced cortical modification would result in a complex combination of both local and global excitation/inhibition phenomena (Borchers et al., 2012). These ideas have motivated a paradigm shift from analyzing just the simulated site to understanding interventions by mapping structural and

functional connectivity of the whole brain network. Nevertheless, the modulatory effects of tDCS on functional brain networks in humans is still not well understood, even though it is key for better understanding the mechanisms of tDCS. Understanding network phenomenon is important for both scientific and clinical reasons. Better understanding may lead to targeted clinical trials and discovery of adjunct therapies, especially important in neurodevelopmental disorders, as is the case in autism spectrum disorder (ASD).

ASD is a complex neurodevelopmental disorder characterized by highly restrictive behavioral interests, and impairments in social interaction and communication (Keown et al., 2017). ASD affects one child out of every 68 children in the U.S. (Baio, 2018), which places heavy burdens on affected individuals, their families, and society. Such statistics highlight the need for interventions targeting young children (Osório and Brunoni, 2019). Common interventions consist of

\* Corresponding author.

E-mail address: [xiaoli@bnu.edu.cn](mailto:xiaoli@bnu.edu.cn) (X. Li).

<https://doi.org/10.1016/j.nicl.2020.102500>

Received 16 January 2020; Received in revised form 5 November 2020; Accepted 7 November 2020

Available online 19 November 2020

2213-1582/© 2020 The Author(s).

Published by Elsevier Inc.

This is an open access article under the CC BY-NC-ND license

(<http://creativecommons.org/licenses/by-nc-nd/4.0/>).

psychoeducational; behavioral approaches and psychotropic interventions (Francis, 2005). However, treatment efficacy is limited and available therapies cannot focus on the relevant brain pathophysiology (MacMaster et al., 2016). There is considerable interest in the potential of using tDCS to ameliorate the deficits of ASD (MacMaster et al., 2016; Kang, 2018; Van Steenburgh et al., 2017). Extensive evidence support the application of tDCS for enhancing cognitive function and motor skills in healthy individuals and as therapeutic intervention for patients with neurological and physiological disorders (Hummel, 2005; Miniussi, 2008), including ASD.

To better understand the changes to resting-state electroencephalograph (EEG) brain networks of ASD children induced by tDCS, we ask two questions. We first ask “how does tDCS change network dynamics?” We hypothesized that tDCS increases flexibility (how often network states change) of brain networks by reconfiguring network connections. Our tDCS-driven network reorganization assumption is inspired by recent works that demonstrate human brain networks would dynamically reorganize before behavior changes (Bassett et al., 2011). Studies have shown that metabolic resource redistribution between strong and weak connections may reasonably support the hypothesis of network reorganization, supporting different network functions (Khambhati, 2015). We test this hypothesis by comparing pre and post-tDCS connectivity networks using a dynamic network analysis method. The method tracks profiles of functional connection strengths over time, which in network theory terminology is collectively referred to as the network’s topological structure (Khambhati, 2015). To compute flexibility, we cluster time points with similar connection strength profiles to obtain network states and find the number of states and how quickly states change over time.

We next asked “how does tDCS change functional connections at specific frequencies?” A recent theoretical framework models brain networks as hierarchical and near-decomposable networks consisting of multiple and partially discrete modules (sub-networks) (Bullmore and Sporns, 2012; Bassett et al., 2011; Zhou et al., 2020). We hypothesized that tDCS changes connection profiles of subnetworks in specific frequencies important to ASD. To test our hypothesis, we identified frequency-specific components of functional brain networks using non-negative matrix factorization (NMF), an unsupervised machine learning technique (Lee and Seung, 1999). Intuitively, NMF could decompose functional brain networks into: (1) additive subnetworks consisting of clusters of graph edges (channel pairs) that interact with each other, and (2) corresponding frequency-specific coefficients that quantify the weight level to which a subnetwork interacts at each frequency (Khambhati et al., 2018a, 2018b; Chai, 2017). This method maps the architecture of subnetworks, showing whether they are local or long-range and shows the frequencies at which subnetworks are active and the relative strength of activity pre- and post tDCS.

## 2. Materials and methods

### 2.1. Participants

In the present study, we recruited thirty-eight participants, which included eighteen participants (eleven males, seven females) who received tDCS stimulation and twenty participants (eleven males, nine females) who received sham stimulation as a control group. Two participants were excluded from the analysis due to excessive noise in the EEG recording during sham tDCS. Therefore, we analyzed data from thirty-six participants, which included eighteen participants (eleven males, seven females; mean  $\pm$  SD age:  $6.5 \pm 1.4$  years) who received tDCS stimulation and eighteen participants (eleven males, seven females; mean  $\pm$  SD age:  $6.7 \pm 1.3$  years) who received sham stimulation. Participants were all diagnosed with ASD by professional psychiatrists in a Chinese hospital based on PEP-III (Chen et al., 2011) and DSM-IV-TR criteria (Sadler and Fulford, 2006).

The research protocol strictly followed safety procedures for non-

invasive brain stimulation (Poreisz et al., 2007; Fertonani et al., 2015) and was approved by the ethics committee of Beijing Normal University. Informed consent was obtained from all parents before the start of the experiment. All protocols of this study conform to the Declaration of Helsinki guidelines.

## 3. Stimuli and procedures

Fig. 1 shows the experimental protocol. For each participant, we recorded 5 min of resting state EEG before (pre-tDCS) and after (post-tDCS) a single session of tDCS (of approximately 20 min) over dorso-lateral prefrontal cortex (FC3); both recordings were performed during an eyes-open resting condition. The experiment was double-blind in design and consisted of two conditions: anodal (18 participants) and sham tDCS (20 participants).

tDCS was delivered by a battery driven constant current stimulator (HuahengJingxin Medical GmbH, Nanchang, China) using a saline-soaked surface sponge active anode. The anode (size =  $30 \text{ cm}^2$ ; current density =  $0.03 \text{ mA/cm}^2$ ) was placed over the dorsolateral prefrontal cortex underneath the EEG cap, through an eyelet in a site corresponding to the FC3 electrode, which was then removed. The cathode,  $30 \text{ cm}^2$ , was placed over the right eyebrow. A constant current of 1 mA was applied for 20 min, with 30 s of fade-in/fade-out. For sham tDCS, the electrodes were located in the same positions as in the active stimulation, but the current was supplied for the first 30 s ramp up, 30 s of stimulation, and then the stimulator was turned off (Gandiga et al., 2006). This procedure ensured that the participants felt the tingling sensation at the beginning of the stimulation. Transient EEG artifacts were observed only during the fade-in and fade-out phases of tDCS stimulation. A similar protocol has been employed in comparable studies (Kunze et al., 2016; Mancini et al., 2016; Kang, 2018; Lauro, 2014). At the end of the experimental protocol, all participants were asked to complete a questionnaire to assess whether the stimulation caused any discomfort (Fertonani et al., 2015) (see **Supplemental Materials**).

## 4. EEG recording and preprocessing

EEG equipment (Electrical Geodesics Inc., Eugene, Oregon, U.S.) was used to record continuous EEG activity before and during tDCS. EEG data were collected using a 128-channel EEG system with sampling rate of 1,000 Hz. Resting-state EEG data were acquired while the children were instructed to sit comfortably and relax. Children were usually accompanied by their caregiver and were in a sound-attenuated, electrically shielded room. A research assistant sat to the side of the caregiver and child and assisted in keeping the children calm and still by presenting a quiet toy to the child if he or she became fussy.

Signals were processed using a 0.1 Hz high-pass analog hardware filter and online re-referenced to the vertex (channel Cz) through Net-Station software (Electrical Geodesics Inc.). Electrode impedances were kept below 50K $\Omega$  in accordance with the impedance values of the high-impedance amplifiers of the recording system (Ferree et al., 2001). Based on the standard International 10–10 system, we selected 62 channels of interest from the 128-channel Geodesic Sensor Net to ensure maximum spatial coverage of the whole brain (including frontal, central, temporal, and occipital).

For each channel, a 0.5 Hz digital high-pass filter and a 45 Hz low-pass filter was applied. Data sampled at 1000 Hz were then resampled with interpolation to 512 Hz (resampling was performed after filtering to avoid aliasing higher frequencies when resampling). Independent components analysis (ICA) was performed on cleaned data using FastICA (Rogasch, 2014) to obtain 62 spatiotemporal features corresponding to independent components (ICs). Then, ICs corresponding to blink/oculomotor, muscle, or transient electrode artifacts were identified via visual inspection and via channel-based scalp topography

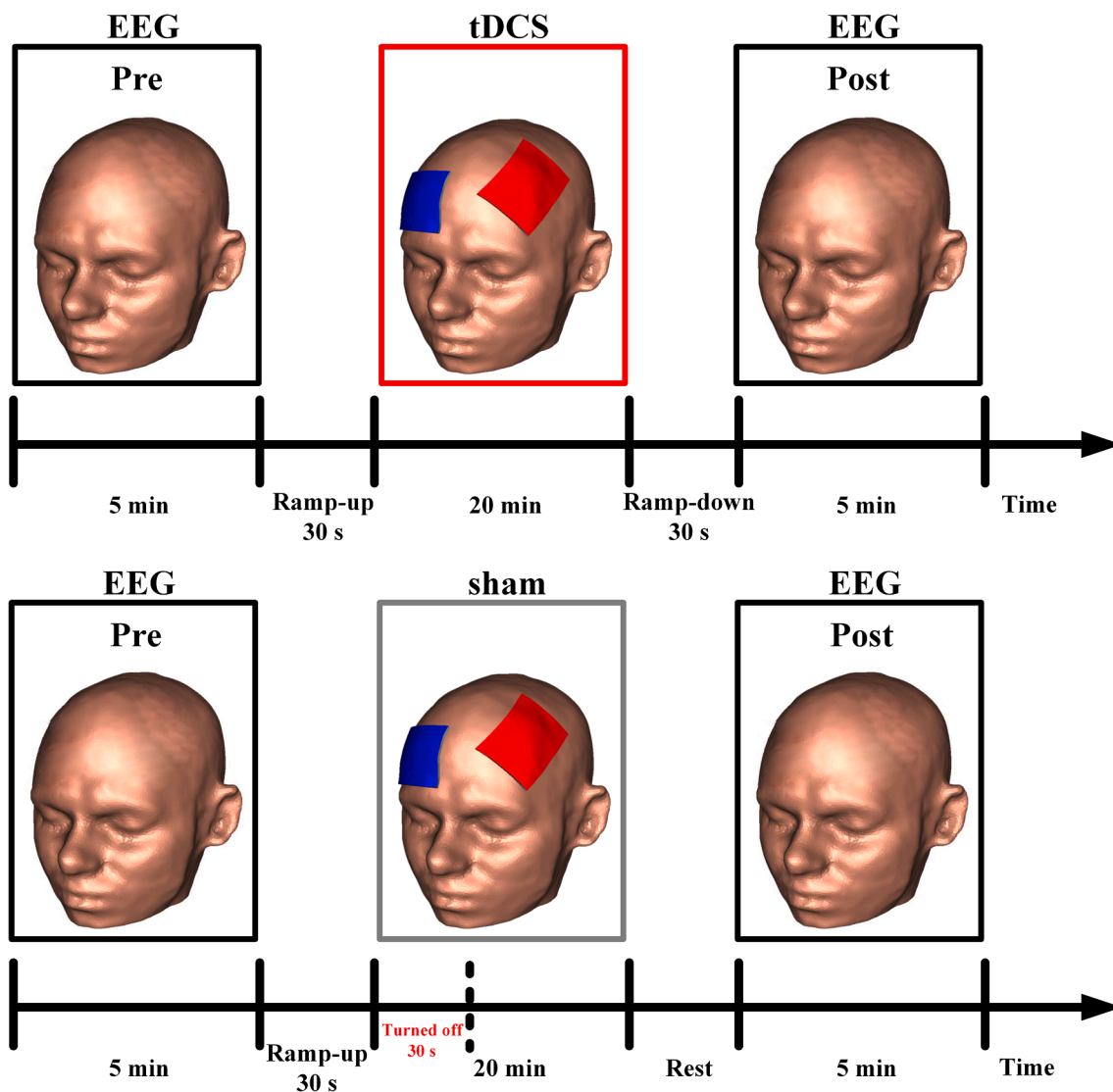


**Fig. 1.** Experimental procedure. Each experimental session consisted of an EEG block before (5 min), during (20 min), and after tDCS (5 min). Each block consisted of a EEG activity recording during a resting state with eyes open. Direct current stimulation (1 mA) was given through two large-sized electrodes placed ( $30\text{ cm}^2$ ) over right eyebrow and the dorsolateral prefrontal cortex.

measures and power spectral density (PSD) measures (median, variance and kurtosis) and subtracted from the data. The EEG data were then re-referenced to the average reference and mean signal and detrended. In order to ensure the quality of the resting-state data, the middle portion of the data (about 2 min in duration) was used for subsequent analysis, since it was less noisy than the entire time series. The EEG data were then cut into 30 non-overlapping segments of 4 s each (Fig. 2A).

## 5. Multi-layer network construction

We constructed a functional network for each 4-s time window using multi-taper coherence estimation. Network connection strength between an electrode pair was defined as the power spectral similarity of signal activity in a specific frequency band. We used custom-built MATLAB scripts along with Chronux software (Bokil et al., 2010) to estimate the multi-taper coherence. Specifically, we first calculated multi-taper coherence with time-bandwidth product of 5 tapers for each spectral frequency, in accordance with a prior study (Kramer et al., 2011). In this study, we adopted the imaginary part of coherence based on multi-taper coherence. For each participant, time window, and frequency band, we computed the multi-taper coherence coefficient

between the preprocessed EEG signals from each pair of electrodes, this process would produce an  $N \times N$  adjacency matrix, where  $N$  is the number of electrodes (62). For each participant, we then combined the individual adjacency matrices at all  $T$  (30) time windows and across all  $F$  frequencies into a multi-layer network, stored in an  $N \times N \times F \times T$  space-frequency-time connectivity tensor  $\mathbf{M}$  (Fig. 2B). We analyze the network in two approaches: temporal dynamics (averaging over frequency) and frequency-specific interactions (averaging over time windows).

## 6. Temporal network analysis methods

### 6.1. Uncovering network states

Our novel approach is based on the dynamic community detection technique (Mucha et al., 2010) to track network states (i.e., temporal changes in network topology) by clustering a configuration-similarity matrix (Chai et al., 2016). First, we construct time-varying network  $\mathbf{A}^*$  by averaging across the frequency dimension (3rd dimension) of tensor  $\mathbf{M}$ , which preserves temporal and spatial patterns. This procedure produces an  $N \times N \times T$  adjacency tensor  $\mathbf{A}^*$  for each participant (Fig. 2C).

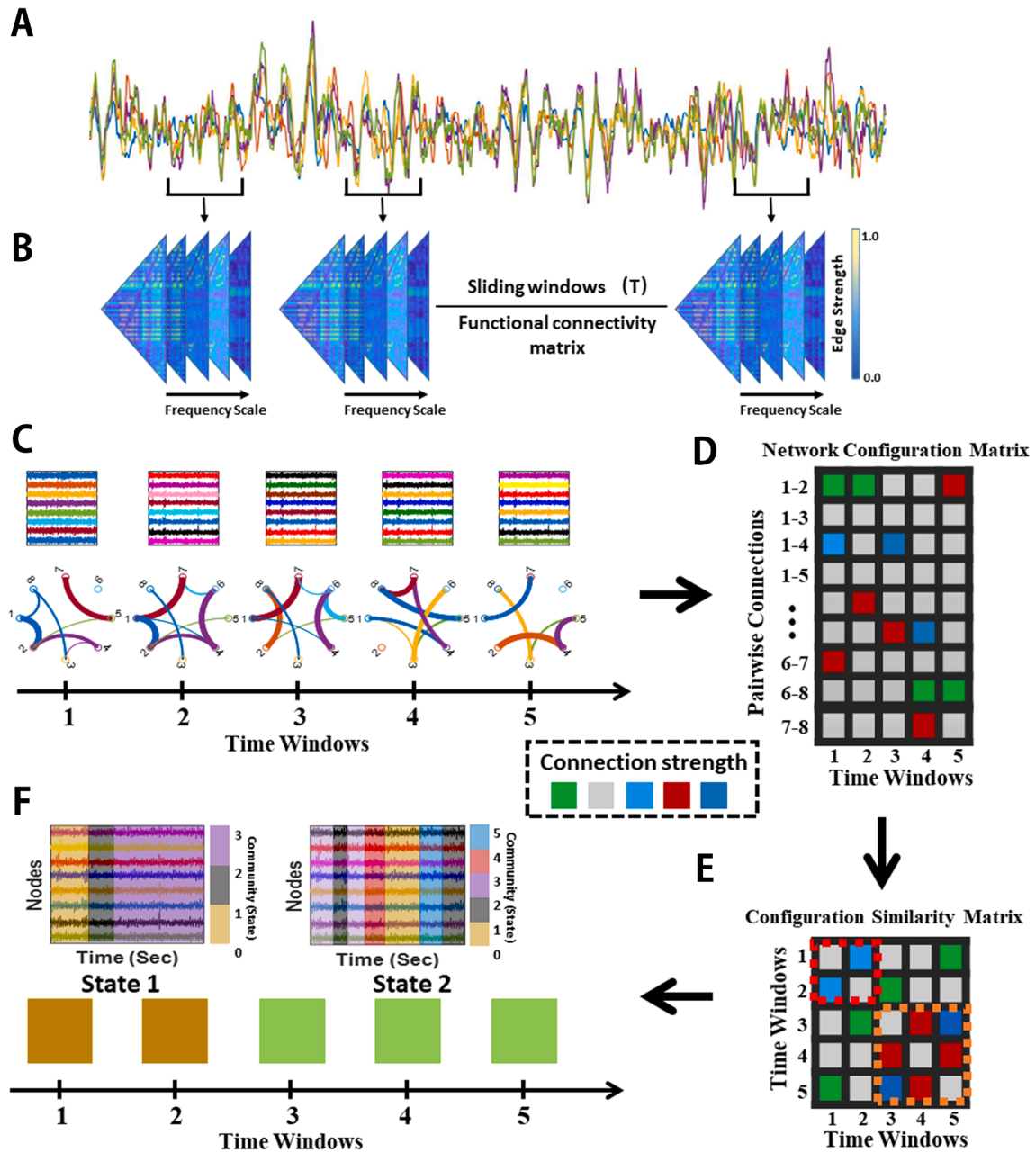


**Fig. 2.** Schematic of experimental procedure for uncovering network configuration states. (A) 62 channels of EEG signals were analyzed, and 120-s time series were extracted and divided into 30 non-overlapping four-second time windows. (B) We construct multi-layer functional networks in each time-window using multi-taper coherence estimation and store results in a tensor with dimensions of frequency, space (channels), and time. (C) We estimate dynamic functional connectivity; color represents arbitrary connection strength. (D) We average over frequency and track all spatio-temporal functional connections; configuration matrix shown, in which each column vector represents the set of all pair-wise connection weights in a 4 s time window. (E) We use Pearson correlation to calculate the similarity between the network topology in each pair of time windows. (F) We map the similarity configuration matrix into communities representing network states by optimizing a modularity quality function.

Second, using the symmetry in tensor  $\hat{A}^*$ , we reorganize the order of entries to construct a network configuration matrix  $\hat{A}$  (Fig. 2D) by unraveling the upper triangle of each  $N \times N$  network connectivity matrix that is a slice of  $\hat{A}^*$ , resulting in a matrix with dimensions  $E = \frac{N \times (N-1)}{2}$  connections by  $T$  time windows. Third, we calculate similarity between time windows in  $\hat{A}$  to obtain a  $T \times T$  configuration-similarity matrix  $S$  (Fig. 2E), using the Pearson correlation coefficient to measure the similarity in pairwise-electrode-coherence ( $E$ -length vector) between each pair of time windows. This configuration-similarity matrix  $S$  is then partitioned into  $n$  communities (Fig. 2F) (representing clusters or network states) by maximizing the modularity index  $Q$  (Newman and

Girvan, 2004) using a Louvain-like locally greedy algorithm (Blondel et al., 2008). A high value of  $Q$  indicates that the temporal connectivity pattern can be aggregated sensibly into different states that exhibit similar connectivity profiles (Bassett et al., 2013).

## 6.2. Temporal network statistics

To examine the relationship among brain regions within a community to characterize the dynamic reconfiguration of spatially distributed neural sources before and after stimulation, our analysis investigated two community metrics, flexibility (Bassett et al., 2011) and module quantity.

“Flexibility” is the number of times that each node changes module allegiance, normalized by the total possible number of changes (Bassett et al., 2011). To measure changes in the composition of modules, we defined the flexibility of a single node  $f_i$  to be the number of times that node changed modular assignment throughout the session, normalized by the total number of changes that were possible. We then defined the flexibility of the entire network as the mean flexibility over all nodes in the network:  $F = \frac{1}{N} \sum_{i=1}^N f_i$ , where  $N$  is the total number of temporal windows. A high value of flexibility means the brain network often switches between modes of activity, i.e. has a high rate of reconfiguration. Module quantity evaluated how much regions communicate with subnetworks in the community structure.

To find substantial changes in metrics across the pre-tDCS and post-tDCS intervals, two-way analysis of variance (ANOVA) was used to analyze the values of flexibility and module quantity before and after tDCS stimulation between sham and stimulation groups. In cases where multiple comparisons were carried out, a Bonferroni correction to the alpha value was used to determine significance. The data met the assumptions of the statistical tests used: data normality were confirmed with Shapiro-Wilk test ( $p > 0.05$ ). Data are expressed as mean  $\pm$  standard error of mean (SEM) unless otherwise specified.

## 7. Frequency-specific network construction

### 7.1. Constructing group-level frequency-specific brain networks

We construct frequency-specific connectivity networks to study the functional interactions between brain areas at distinct frequencies

before and after tDCS intervention. To construct a frequency-specific network, we average across time the coherence values of connectivity tensor  $\mathbf{M}$  (i.e., mean of the 4th dimension). This produces an  $N \times N \times F$  adjacency tensor  $\mathbf{B}$  for each EEG session of each participant. Then, the three-dimension tensor  $\mathbf{B}$  were converted to two-dimensional configuration matrix  $\hat{\mathbf{B}}$ , which arrange all pair-wise edge weights across  $F$  frequencies by unraveling the upper triangle of each frequency slice of  $\mathbf{B}$  into a column vector. Thus,  $\hat{\mathbf{B}}$  has dimensions  $E \times F$ , and we have one such matrix per EEG recording session and participant.

Next, we construct a group-level matrix  $\mathbf{V}$  for identification of group-level network components across all  $S$  participants and four EEG recordings (i.e., pre- and post- tDCS and sham stimulation). We concatenate the single participant network configuration matrices  $\hat{\mathbf{B}}$  across all participants and all EEG recordings, making  $\mathbf{V}$  size  $E \times (4FS)$  (Fig. 3A).

### 7.2. Learning functional subnetworks via NMF

To identify frequency-specific patterns in brain networks, we apply non-negative matrix factorization (NMF) (Lee and Seung, 1999), an unsupervised machine-learning algorithm, on group-level matrix  $\mathbf{V}$ . This technique allows us to approximately decompose the group-level network into topological subnetworks (Fig. 3B) and corresponding network coefficients whose strength vary over frequency bins (Fig. 3C). Mathematically, NMF is a multivariate-decomposition technique that approximates a data matrix  $\mathbf{V}$  (here, size  $E \times (4FS)$ ) as the product of two non-negative matrices,  $\mathbf{W}$  (size  $E \times k$ ) and  $\mathbf{H}$  (size  $k \times (4FS)$ ).

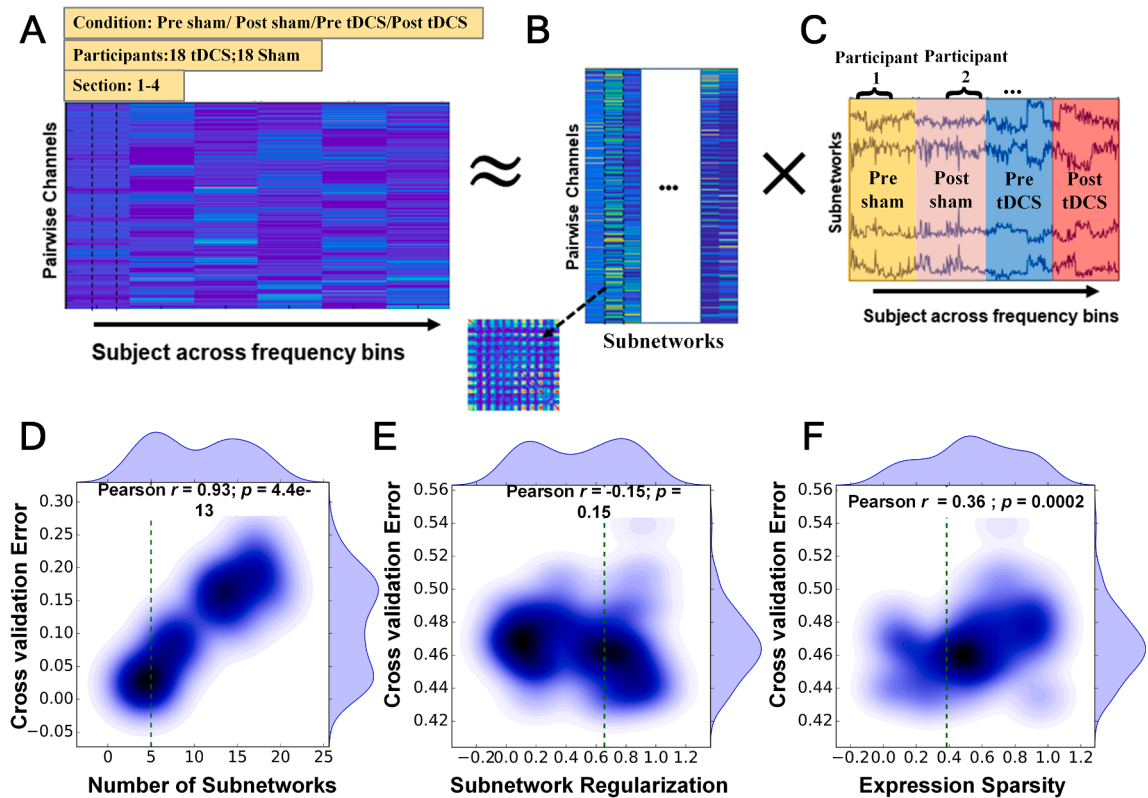


**Fig. 3.** Learning frequency-specific subnetworks of the brain network. (A) We concatenated all channel pairs over recording time points, participants, and sessions, and we generated a single frequency-dependent network configuration matrix  $\mathbf{V}$ . We then applied nonnegative matrix factorization, which decomposed  $\mathbf{V}$  into two matrices: one represents (B) spatial architecture; and the other (C) a participant-and-session-specific spectral profile. NMF-based network components detection requires optimizing three meta-parameters: (D) the number of network components; (E) the spectral sparsity of network component expression; and (F) the regularization parameter for network component edge weights. The kernel-density estimates of each parameter along with cross-validation error are shown by contour plots, where darker shades indicate higher probability mass. The best meta-parameters were chosen as the average values that produce minimum cross-validation error in the sample distribution, indicated by the green dashed line. (For interpretation of the references to color in this figure legend, the reader is referred to the web version of this article.)

$k \in \left[ 2, \min \left( \frac{N \times (N-1)}{2}, 4FS \right) - 1 \right]$  is the number of patterns in the decomposition. We solve the matrix-factorization problem  $V \approx WH$ , with constraints  $W \geq 0, H \geq 0$  by optimizing the following cost function  $f$ :

$$f(W, H) = \min_{W, H} \frac{1}{2} \left\{ \|V - WH\|_F^2 + \alpha \|W\|_F^2 + \beta \sum_{j=1}^{TS} \|H(:, j)\|_F^2 \right\} \quad (1)$$

with  $W \geq 0, H \geq 0$

where  $\beta$  is a penalty weight that enforces sparsity on the frequency-specific coefficients  $H$ , and  $\alpha$  is a regularization parameter that provides an upper bound on the connection strength within the spatial patterns  $W$  (Kim and Park, 2011). To solve the NMF, we performed 100 iterations using block-pivoting alternating least squares with non-negative constraints (Kim et al., 2014). We randomly initialized the two matrices ( $W$  and  $H$ ) from a uniform distribution on the interval  $[0, 1]$ .

The selection of parameters  $k, \beta$ , and  $\alpha$  is crucial when applying NMF to obtain networks. Here, we used a random-sampling strategy where we ran the NMF algorithm 1,000 times for different *meta*-parameter sets. This scheme has been shown to be effective in optimization of high-dimensional parameter spaces (Khambhati et al., 2018). In each set,  $k$  was randomly selected between 2 and 20,  $\beta$  was randomly selected from 0.01 to 1, and  $\alpha$  was randomly selected from 0.01 to 1. We evaluated fit performance based on five-fold cross-validation. Four folds were used to extract subnetworks and the one held-out fold was used to calculate the cross-validation error ( $\|V - WH\|_F^2$ ). The optimal parameter set yielded subnetworks that minimized the objective function  $\|V - WH\|_F^2$  and reliably spanned the observed network topology space (Khambhati et al., 2018). Based on these criteria, we chose the parameter set  $(\bar{k}, \bar{\beta}, \bar{\alpha})$  that showed a low residual error according to our scheme (Fig. 3D-F).

Due to the NMF algorithm random initialization problem, we use consensus clustering to combine estimated patterns from multiple runs of NMF method. The consensus clustering method was designed for finding the consensus over multiple randomly-initialized runs of clustering algorithms (Monti et al., 2003). The consensus clustering procedure we adopted (Greene et al., 2008) contained the following steps: (i) run NMF  $R$  times on network matrix  $V$ , (ii) concatenate subnetwork matrix  $W$  across  $R$  runs into an aggregate matrix with dimensions  $E \times (R\bar{k})$ , (iii) apply NMF with parameter set  $(\bar{k}, \bar{\beta}, \bar{\alpha})$  on the aggregate matrix to determine a final  $W$  and  $H$ . In the present study, we set  $R = 100$ .

### 7.3. Test-retest reliability of connectivity patterns

To assess the reproducibility of connectivity patterns, we measure the extent to which the network pattern's edge weights fitted from the first dataset predicts the edge weights fitted from the second dataset. We first applied NMF with the optimized parameter set to two different datasets ( $\hat{V}_1$  and  $\hat{V}_2$ ), giving two subnetwork matrices ( $W_1$  and  $W_2$ ). The columns of  $W_1$  may not necessarily have the same order as the columns of  $W_2$ . To rearrange connectivity patterns of the second dataset so that they correspond to the first dataset, we then sought a mapping  $X_{ij}$  from the subnetwork  $W_1^i$  to subnetwork  $W_2^j$ , where  $W_1^i$  represent the  $i^{\text{th}}$  subnetwork from the first dataset,  $W_2^j$  represent the  $j^{\text{th}}$  subnetwork from the second dataset, and  $X$  is a Boolean matrix which assess whether  $W_1^i$  is uniquely assigned to  $W_2^j$ . To identify a unique  $X$ , we used the Hungarian algorithm to minimize the cost function  $\sum_i \sum_j X_{ij}$  (Kuhn, 1955). We first calculated an optimal assignment between connectivity patterns of the two datasets. We then quantified the similarity of the connectivity patterns between assigned subnetwork pairs ( $i, j$ ) by calculating the Pearson correlation coefficient (Khambhati, 2018). This approach enables us to evaluate the reproducibility of each network component depending on the magnitude of the Pearson correlation

similarity measure relative to accidental expectation (Khambhati et al., 2018).

### 7.4. Frequency-specific subnetwork statistical evaluation and network visualization

The outcome of NMF consisted of two matrices. One matrix represents spatial brain structure. We reorganized the rows and columns of each subnetwork's  $N \times N$  matrix  $W$  that contained spatial brain structure, and we then visualized it as a ring graph. The other matrix contains the participant-specific spectral profile for each subnetwork, we calculated the participant- and condition-specific spectral energy or peak frequency to characterize subnetworks' differences.

To facilitate frequency-specific network component comparisons in frequency-specific metrics (spectral power or alpha peak frequency) across the pre-tDCS and post-tDCS intervals, two-way analysis of variance (ANOVA) was used to analyze the effects before and after tDCS stimulation on frequency-specific metrics between sham and stimulation groups for each network component. In cases where multiple comparisons were carried out, a Bonferroni correction to the alpha value was used to determine significance. The data met the assumptions of the statistical tests used: data normality were confirmed with Shapiro-Wilk test ( $p > 0.05$ ). All statistical analyses and graphical representations were produced using GraphPad Prism 8.0 Software. Data are expressed as mean  $\pm$  standard error of mean (SEM) unless otherwise specified.

## 8. Results

### 8.1. Tolerability & safety

Immediately following stimulation, participants completed an adapted form of the side-effect questionnaire. This questionnaire asked about two commonly-reported side effects (tingling, burning sensation) as well as an "other" discomfort category that allows participants to describe experiences/sensations not otherwise covered. There were no serious adverse events and no participants withdrew, suggesting that tDCS met basic safety parameters. Tolerability was comparable between active and sham tDCS with 1 mA intensity ( $t$ -test of combined frequency of all three sensations comparing between groups,  $p > 0.9$ ). Tingling was rarely endorsed (0% in active; 5% in sham). Burning sensation and other discomfort were not endorsed (0% in active; 0% in sham). One participant from the sham group reported feeling tingling but did not provide a severity rating. In summary, there were no significant differences between active and sham groups in reports of side effects across the entire sample (Supplemental Materials, Table 1).

TDCS is a non-invasive method of brain stimulation which is generally regarded as safe and well tolerated. Studies have examined the safety and tolerability of tDCS and blinding of tDCS studies at stimulation intensities of 2 mA or greater, up to 3 mA (Reckow, 2018; Paneri, 2016). Empirical findings suggest similar side effect profiles between active and sham tDCS (Giordano, 2017; Borckardt, 2012). Given the

**Table 1**

A list of  $p$  values is reported resulting of flexibility and Module quantity from the post-hoc planned comparisons (Bonferroni corrected). Estimates of  $P$ -values, Bonferroni corrected  $P$ -values (Adj.  $P$ .), 95% confidence intervals (CI) are reported.

	Flexibility			Module quantity		
	P-value	Adj. P.	CI	P-value	Adj. P.	CI
Pre-sham vs. Pre-tDCS	>0.12	0.94	[-0.2, 0.1]	>0.12	0.57	[-0.1, 0.5]
Pre-Sham vs. Post-Sham	>0.12	0.15	[-0.1, 0.01]	>0.12	0.91	[-1.1, 0.6]
Pre-tDCS vs. Post-tDCS	<0.03	0.04	[-0.3, -0.003]	<0.03	0.02	[-1.8, -0.1]

current study's focus on children, a constant current of 1 mA was applied to the active group, with 30 s of fade-in/fade-out. This setting ensures consistency of safety and tolerability between the active and sham groups. The protocol required study team members to immediately alert the senior author (LXL) to any serious adverse events; none were reported by participants or observed by the study team members.

### 8.2. Network dynamics change with stimulation

We first asked, "how does tDCS change network dynamics?" To answer the question, we applied a recent approach to detect network states, defined by unique patterns of channel-channel network connectivity among  $T = 30$  time windows (see Materials and methods; Fig. 2C-F) (Khambhati, 2015). We define a network state as a collection of all time windows that exhibit similar functional connectivity patterns, more formally referred to as "network geometry" in the network science literature (Khambhati, 2015; Khambhati et al., 2018). To measure geometric similarity, we computed the Pearson correlation coefficient among configuration vectors (vectors of all pairwise electrode coherence values) (Fig. 2D). This procedure produced a symmetric  $30 \times 30$  configuration-similarity matrix (Fig. 2E). We then applied a community detection method to the configuration-similarity matrix (Fig. 2F, see Materials and methods). The community detection approach assigns each time window to a network community (or network state), and each community/network state consists of time windows which exhibit similar network topologic. We found that the brain network transitions through a diversity of network states before and after tDCS.

In the first main ANOVA, the results showed a statistically significant effect on the main factor of time (post-tDCS and pre-tDCS) in flexibility:  $F(1, 17) = 13.38$ ;  $p < 0.0017$ , suggesting that the flexibility value significantly increased following the tDCS. The results also showed a statistically significant effect on the main factor of group (tDCS versus sham) in flexibility:  $F(1, 17) = 4.625$ ;  $p < 0.044$ , suggesting that the flexibility changes induced by tDCS were not merely a placebo effect. The interaction between time and group was not significant ( $F(1, 15) = 3.74$ ;  $p = 0.072$ ).

In the second main ANOVA design showed similar a significant changes in module quantity that include time ( $F(1, 17) = 7.18$ ;  $p < 0.014$ ) and group ( $F(1, 17) = 10.59$ ;  $p < 0.0042$ ) factors. The result implied the module quantity value would significantly increase following the tDCS stimulation. The interaction between time and group was not significant ( $F(1, 15) = 3.04$ ;  $p = 0.1$ ).

We also performed the post-hoc comparison (Fig. 4). We compared the baseline levels of the two condition-specific group (pre-tDCS vs. pre-sham), and we did not observe the significant difference in flexibility ( $p = 0.94$ ) and module quantity ( $p = 0.57$ ) between pre-sham and pre-tDCS. This means that there is no difference at baseline level. Then, we evaluated the post-pre change of flexibility (Fig. 4A) and module

quantity (Fig. 4B) for each treatment group (i.e., tDCS group and sham group). The result showed that the tDCS-induced changes of flexibility and module quantity is significantly higher than sham group ( $p < 0.05$ ), it strongly suggested that tDCS could significant increase the flexibility and module quantity of brain network in ASD children (see Table 1 for a detailed list of  $p$  value found).

To conclude, our result demonstrated that tDCS had a strong immediate effect on the regulation of brain network, significantly increasing the switching speed of network states; the sham stimulation did not show any significant modulation of network temporal characteristics ( $p > 0.12$ ).

### 8.3. Frequency-dependent network components

We next asked "how does tDCS change functional connections at specific frequencies?" To analyze interactions in the network at specific frequencies, we constructed group-level (pooled data among participants) frequency-dependent brain networks, represented as matrix  $V$  with dimensions  $\frac{N \times (N-1)}{2} \times (4FS)$  (Fig. 3A) (see Methods and materials for details), where  $N = 62$  channels,  $F = 689$  frequency bins (2 to 45 Hz with step 0.0625 Hz),  $S = 18$  represent participants, and four is the number of EEG recording time points. Here, we averaged across time windows. We retained and analyzed all pairwise connection weights between channels without applying any threshold. This  $V$  matrix was then used as input to the non-negative matrix factorization algorithm and subsequent processing.

We applied NMF to the group-level connectivity network (Fig. 3A). The parts-based decomposition algorithm decomposed the network edges into additive functional subnetworks (i.e., frequency-specific network patterns; Fig. 3B) and accompanying frequency-specific expression coefficients over participants (Fig. 3C) (Chai, 2017; Khambhati et al., 2018). Each subnetwork was represented by a  $62 \times 62$  adjacency matrix, and each subnetwork's participant-specific frequency coefficients were composed of a vector of length 49,608 (i.e. 4FS). Thus, the subnetworks comprised the spatial topological network components, and the expression frequency domain coefficients quantified their synchronized interactions in particular frequency bands. A critical part of using NMF is the optimization of meta-parameters (i.e., number of subnetworks,  $k$ ; spectral profile sparsity of subnetwork expression,  $\alpha$ ; and regularization parameter for subnetwork edge weights,  $\beta$ ) to avoid overfitting. We used a five-fold cross-validation scheme, and we minimized the average cross-validation error on held-out participants. The optimal number of subnetworks was found to be five, the spectral profile sparsity to be 0.65, and the regularization parameter for the subnetwork edge weights to be 0.39 (Fig. 3D-F; see Materials and methods). We reordered the channels to group together brain regions and then visualized the resulting adjacency matrices as ring graphs, along with their corresponding spectral profiles. We categorized the extracted network

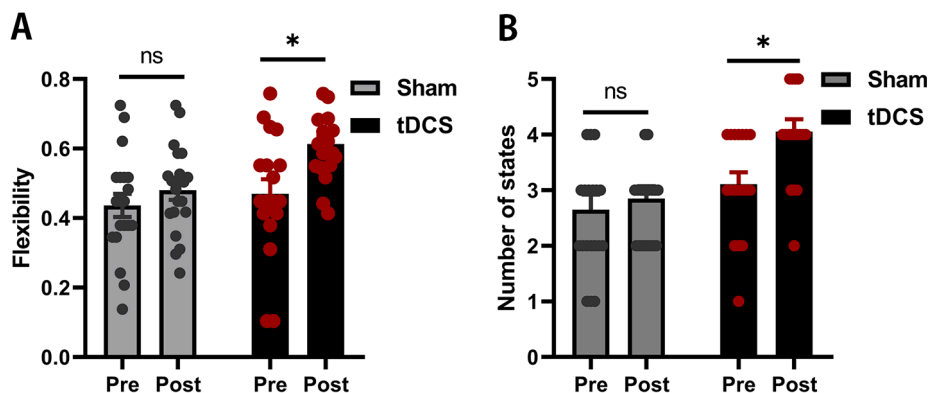


Fig. 4. Network state temporal characteristics. (A) Mean  $\pm$  SEM of flexibility before and after intervention for each treatment group. (B) Mean  $\pm$  SEM of module quantity before and after intervention for each treatment group. \*  $p < 0.03$ . ns, no significant.

components into two groups based on the characteristics of spectral profiles for statistics, with (Pattern A, B; Fig. 5) and without clear peak frequency (Pattern C-E; Fig. 6) among spectral profiles.

We subsequently explored the topology of the resulting network components, and each with participant-specific spectral profiles (Fig. 5). Specifically, for Pattern A and B, the participant-averaged spectral profiles were band-limited to a certain frequency range, which moreover showed a consistent peak frequency across participants. This suggests that these subnetworks represent frequency-specific rhythmic directed interactions between key regions in this tDCS-relevant large-scale network. Pattern A reflected predominantly inter-hemispheric connections from left prefrontal lobe to right posterior occipital lobe (Fig. 5 A), with a median peak frequency at 13 Hz. However, neither the group (real versus sham):  $F(1, 17) = 2.99, p = 0.1$ , nor the time (before versus

after):  $F(1, 17) = 0.712, p = 0.4$  were significant. For the post-hoc comparisons, we did not observe a significant difference in peak frequency between pre- vs. post-sham stimulation ( $p > 0.1$ ) and pre- vs. post-tDCS ( $p > 0.1$ ).

Pattern B reflected predominantly homotopic inter-hemispheric connections from left temporal lobe to right temporal lobe, with a median peak frequency at 10 Hz. We observed a significant changes on time ( $F(1, 17) = 12.27, p = 0.0027$ ) and group factor ( $F(1, 17) = 4.65, p = 0.0457$ ). The result implied the peak frequency value would significantly shift toward higher frequency following the tDCS stimulation. The interaction between time and group was not significant ( $F(1, 15) = 3.04; p = 0.1$ ). For the multiple comparisons, we observed a significant increase in peak frequency between pre-tDCS and post-tDCS ( $p < 0.01$ ). In the other hand, we did not observe a significant change between pre-

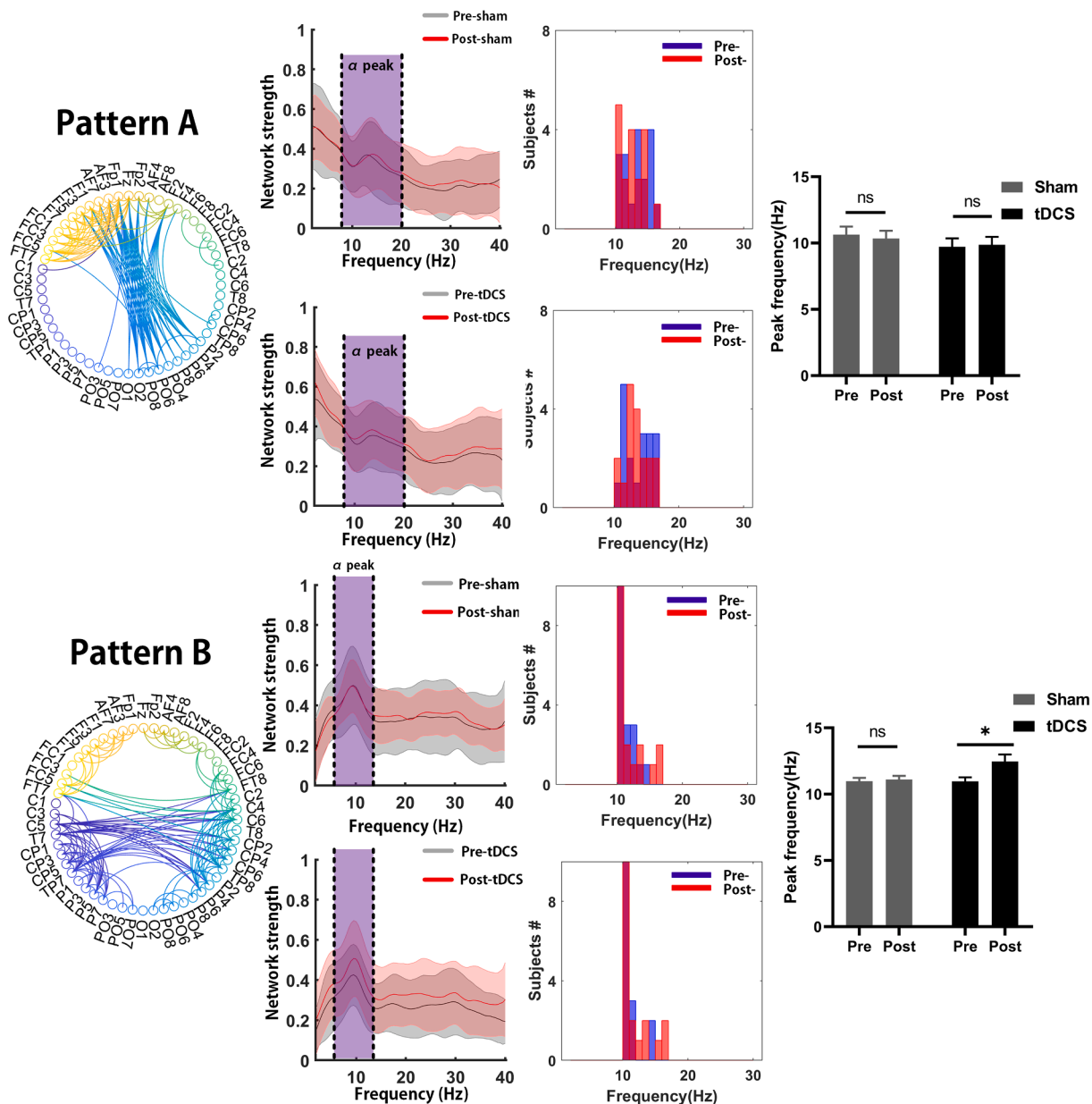


**Fig. 5.** Subnetworks obtained from NMF show frequency- and region-specific interaction. Leftmost panels for each subnetwork shows topological architecture in a ring graph, where edges were thresholded at the 90th percentile for visualization. The spectra show the median spectral profile across participant. The histograms show the distribution of the participant-specific peak frequency before and after intervention for each treatment group. The red spectrum is the average of post-stimulation. The purple shade between the dotted lines indicate the stimulation-induced change of spectrum, and is the area to be statistical analysis. Rightmost panels show statistics result of tDCS-induced changes of peak frequency for each treatment group. \*  $p < 0.03$ . ns, no significant. (For interpretation of the references to color in this figure legend, the reader is referred to the web version of this article.)

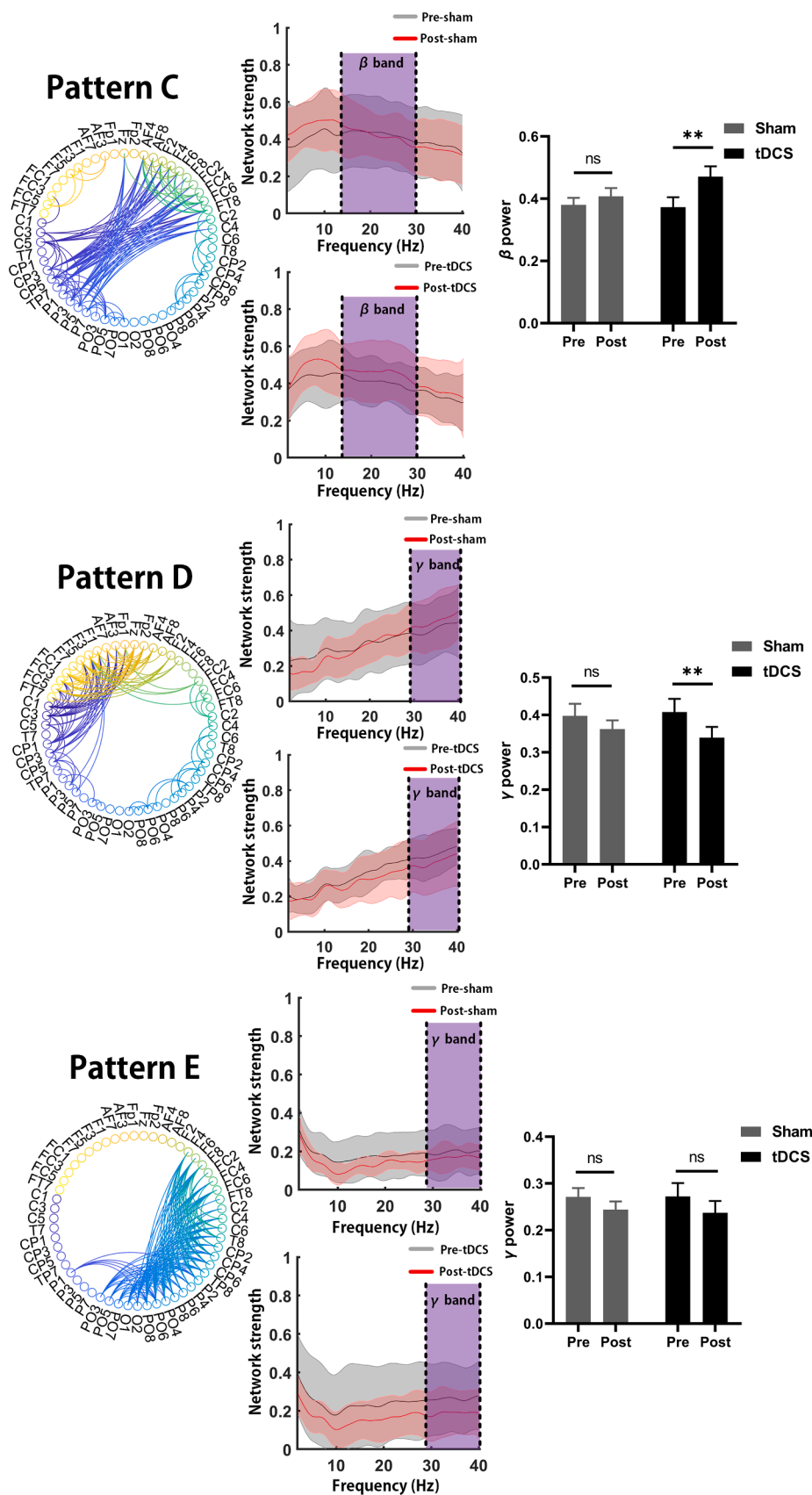


**Fig. 6.** Subnetworks obtained from NMF show frequency- and region-specific interaction. Left panel for each subnetwork shows topological architecture in a ring graph, where edges were threshold at the 90th percentile for visualization. Middle panel for each subnetwork shows the median spectral profile across participant. The gray spectrum is the average of pre-stimulation. The red spectrum is the average of post-stimulation. The purple shade between the dotted lines indicate the stimulation-induced change of spectrum. Rightmost upper panels show mean  $\pm$  SEM of frequency power before and after intervention for each treatment group. Rightmost panels show statistics result of tDCS-induced changes of band power for each treatment group. \*  $p < 0.03$ . \*\*  $p < 0.002$ . ns, no significant. (For interpretation of the references to color in this figure legend, the reader is referred to the web version of this article.)

sham and pre-tDCS ( $p > 0.6$ ). Together, the result indicated that tDCS could modulate the homotopic interhemispheric pattern with shifting alpha peak frequency towards higher frequencies.

We next investigated the network components which had a tDCS-induced changes of coherence over more broadband spectral profile (Fig. 6). Pattern C which predominantly interconnecting right temporal lobe and left temporal lobe showed somewhat more variability in their  $\beta$  band across subjects after tDCS. The main ANOVA result showed a significant effect on the main factor: time ( $F(1, 17) = 13.44, p = 0.0019$ ), but we did not observe a significant effect on the group factor ( $F(1, 17) = 1.29, p = 0.27$ ). For the multiple comparisons, we observed a significant difference in beta power between pre-tDCS and post-tDCS ( $p < 0.01$ ).

Pattern D was a tDCS-induced local pattern, with a robust and relatively dense pattern of connectivity over left prefrontal areas. The main ANOVA showed a significant effect on the main factor: time ( $F(1, 17) = 9.871, p = 0.0059$ ), but we did not observe a significant effect on the group factor ( $F(1, 17) = 0.055, p = 0.81$ ). For post-hoc comparisons, we observed a significant difference in gamma power between pre-tDCS and post-tDCS ( $p < 0.03$ ). The result implies a significant and dramatic power decrease in local gamma over left prefrontal areas after tDCS treatment.

Pattern E was somewhat spatially more localized, with predominantly right intra-hemispheric short-range connections mainly distributed in posterior occipital and posterior temporal regions. Neither the group (real group versus sham group):  $F(1, 17) = 2.99, p = 0.1$ , nor the time:  $F(1, 17) = 0.712, p = 0.4$  were significant. For the post-hoc comparisons, we observed a broadband decrease of coherence for frequencies from 30 Hz to 40 Hz in the post-tDCS period (red line), compared with the baseline period (grey line), but not statistically significant ( $p > 0.05$ ).

Through all the patterns, another observation is that tDCS made oscillations more harmonic (indicated by a sharpening of the frequency spectrum with clearer peaks), indicating synchronization during tDCS (see Table 2 for a comparison of the standard deviation), consistent with previous research results (Kunze et al., 2016). Here, more harmonic oscillations means a sharpening of brain areas' frequency spectrum with lower standard deviation.

In summary, tDCS significantly modulated the homotopic interhemispheric pattern from left temporal regions to right temporal regions, with shifting alpha peak frequency towards higher frequencies (Pattern B). Overall, subnetwork-specific median peak frequencies ranged from the lower end of the theta range (5 Hz) to the lower end of the beta range (20 Hz). In addition, tDCS significantly enhanced synchronization over heterotopic interhemispheric patterns from right temporal region to left temporal region (Pattern C). Meanwhile, tDCS significantly weakened synchronization over localized frontal regions in the left hemisphere for gamma band (Pattern D). In conclusion, tDCS could modulate ASD-related functional connectivity by inter-hemispheric over-synchronization and local under-synchronization within higher frequency bands (alpha, beta and gamma).

## 9. Discussion

In the present study, we use EEG recordings to measure pre- and post-stimulation brain connectivity changes induced by anodal tDCS. The

**Table 2**  
Baseline in mV (standard deviation in mV) of the areas following tDCS.

Pattern #	Pre-sham	Post-sham	Pre-tDCS	Post-tDCS
A	216.37 (93.5)	240.89 (80.3)	201.22 (83.7)	223.98 (66.4)
B	148.10 (55.7)	178.44 (60.4)	135.37 (61.0)	167.02 (53.6)
C	227.36 (53.2)	253.32 (51.9)	234.61 (66.4)	266.54 (56.4)
D	179.44 (61.2)	131.30 (60.6)	189.31 (75.0)	138.33 (58.9)
E	120.24 (61.4)	90.80 (47.7)	138.63 (82.3)	111.06 (38.9)

aim was to evaluate the tDCS-induced effect on the brain functional connectivity in persons with autism. The first interesting finding was that rapid network reconfiguration of dynamic network communities were observed (revealed by increasing network flexibility) following tDCS. The second result was that tDCS-induced frequency-specific subnetworks, as a way to index local and global information processing, highlight the fundamental modulation in the modular architecture of functional connectivity patterns within higher frequency bands (alpha, beta, and gamma). Specifically, a connectivity increase was observed over inter-hemispheric areas within alpha (8–13 Hz) band following tDCS.

### 9.1. Reconfiguration of network after tDCS

Regarding the first result, we investigated network reconfigurations from resting state EEG following tDCS using dynamic community detection (Mucha et al., 2010) without prior knowledge of specific topological structure (Khambhati, 2015). Changes in functional network organization before and after stimulation were characterized using metrics from network science: network flexibility, a metric that describes how often each node changes the community to which it is allied (Bassett et al., 2011). This analysis captures whether stimulation drives certain brain regions to cohere with different communities in a manner that is different from their community participation prior to stimulation. We observed a significant increase in flexibility after tDCS. Our results suggest a rapid reconfiguration of the resting community organization following tDCS stimulation, rather than enhancement of a single community. The results extend previous research that has found network flexibility successfully characterizes large-scale functional differences in executive function (Braun, 2015) and mood (Betzel et al., 2017).

Most previous neuroimaging studies (Klein et al., 2016; Palomar-García et al., 2017), which address the connectivity of functional networks, focus on static functional connectivity and did not specifically target the nonstationary nature of the functional connectivity that contains a wealth of information (Li et al., 2020). Our results showed a profound and noticeable dynamic integration of brain functional systems, more frequent state changes after tDCS compared to before (higher flexibility). Our results suggest that tDCS is capable of reconfiguring the brain network of children with autism to change states more often. One compelling current theory posits that even small and short-term changes in connectivity are able to initiate switching of network dynamics (Hansen et al., 2015). Greater switching of network states illustrates enhanced brain plasticity (Li et al., 2020). Our results provide evidence for tDCS-induced brain plasticity, and the experiment may help to establish effective tDCS modulation therapy strategies for children with ASD and other neurological disorders.

### 9.2. Subnetworks show frequency-dependent functional interaction changes after tDCS

Regarding the second finding, we investigate frequency band-specific communities (subnetworks) from a concatenated functional network of all the subjects and four EEG recording time points (pre-sham, post-sham, pre-tDCS and post-tDCS) in frequency points (scales) using the NMF technique. Data-driven decomposition of the overall network into smaller subnetworks revealed several spatially constrained components, corresponding to local and/or long-range interactions (Schoffelen et al., 2017). The clear frequency-resolved profile displayed by some of these connectivity patterns indicate that the interaction is modulated by rhythmic synchronization between regions. Our results showed that there was an increasing trend in the alpha band global inter-hemispheric connectivity after tDCS, the frequency distribution of rhythmic synchronizations was sharpened and peak frequency slightly shifted towards higher frequencies within alpha band (pattern B). Another observation was that there was a significant decrease in the gamma band (30–40 Hz) connectivity over local intra-hemispheric parts

of the left prefrontal-temporal region after tDCS stimulation (pattern D).

The present findings agree with recent literature reporting an increase of alpha band after tDCS (Vecchio et al., 2016). They also agree with studies reporting a higher beta coherence in the sensorimotor cortex underlying anodal tDCS (Notturmo et al., 2014). Furthermore, a previous study has demonstrated that, in the resting brain, tDCS alters ongoing brain activity, specifically in the alpha band rhythm (Spitoni et al., 2013).

While low-frequency alpha rhythms are supposed to reflect the regulation of global cortical arousal (Klimesch, 1999). Such lower EEG frequency activity, ranging across delta, theta and alpha, has been interpreted as global activity arising from long-distance coordination of synchronized neural firing in disparate brain regions (Brunel and Wang, 2003). Changes in power in high frequencies, such as beta and gamma, have been used to infer local dynamics arising from the synchronization of populations of neurons (Klimesch, 1999).

An involvement in the alpha rhythm after the application of anodal tDCS, as observed in our study, has been reported in other recent works. Alpha frequency modulations, in terms of an increase in the peak alpha frequency (Amatachaya, 2015) and an increase in alpha frequency power (Pellicciari et al., 2013; Mangia et al., 2014), have been reported during and post-anodal stimulation, emphasizing the role this band plays as a cortical marker of the neuromodulatory effects induced by tDCS. Recent studies suggest that an increase in EEG spectral coherence values can be interpreted as an enhancement of the linear functional connections and information transfers (i.e., functional coupling or binding), reflecting the interaction of individual cortical structures. Increased coherence in alpha or in faster EEG frequencies reflects a greater facilitation, or functional connectivity (Vecchio et al., 2016).

Interestingly, in our previous study (Zhou et al., 2020), we found that the brains of children affected by ASD were characterized by a general trend toward long-range under-connectivity within alpha band, particularly in interhemispheric connections, combined with short-range over-connectivity within beta band. The results were also supported by other studies (O'Reilly et al., 2017). A substantial body of research results have shown that the ASD brain is characterized by a pattern of short-range over-connectivity (Belmonte et al., 2004) and long-range under-connectivity (Geschwind and Levitt, 2007), or even global under-connectivity (Just et al., 2004). The clear lateralization in the local pattern of connections support the notion that tDCS-induced changes in functional connectivity potentially bias (e.g., activate or deactivate) certain functional networks (Kunze et al., 2016). A targeted bias of functional networks might explain the numerous positive effects that tDCS has on neurological and psychiatric diseases (Fregni and Pascual-Leone, 2007; Lindenberg et al., 2010). The atypicalities in functional connectivity patterns in individuals with ASD could be regulated by tDCS stimulation. The results provide evidence for tDCS-induced brain plasticity, and the modulation may indicate that tDCS is feasible in children with ASD and might be used as a novel rehabilitation technique.

## 10. Experimental design considerations

Our experimental design did not employ cathodal tDCS over left DLPFC, instead, we placed the anodal tDCS over left DLPFC to investigate the neurostimulation effect on brain networks, based on the rightward lateralization hypothesis of ASD (Floris, 2016).

The abnormal function of specific brain areas (e.g., amygdala and fusiform gyrus) which participate in face processing and social cognition, have been consistently demonstrated to be hypo-activation in individuals with autism spectrum disorder (Hubl, 2003; Corbett, 2009). The hypo-activation of these specific brain areas, found especially in the left hemisphere, called rightward lateralization, was commonly found evidence in individuals with autism (Cardinale et al., 2013). Several research results showed that anodal tDCS over the left hemisphere (as employed in the present study) might be useful for improving the hypo-

activation of atypical rightward lateralization and cortical plasticity in autistic individuals (Amatachaya, 2014). Our findings of tDCS-induced modulation of alpha band inter-hemispheric connection strongly support these research results, which suggest anodal tDCS over the DLPFC could ameliorate rightward lateralization. Meanwhile, a recent study also suggests that anodal tDCS could possibly modify cortical connectivity more effectively with respect to cathodal tDCS (Vecchio et al., 2016), which coincided with the aim of our present study to test the neuromodulation effect over stimulated connectivity.

The absence of a control group (TD) could represent a limitation of the experimental paradigm. Nevertheless, it should be emphasized that the aim of the present study was to investigate the connectivity difference before stimulation and after stimulation. The sham condition helps us rule out a placebo effect; the lack of a control group (TD) does not seem to be of remarkable importance. Furthermore, it is very difficult to perform tDCS stimulation on typically developing children in a practical experiment. Nevertheless, further studies should evaluate modulation with a control group comparison.

## 11. Limitations

Limitations exist in the current study. First, the experimental design only contained a single tDCS group and a single sham group, without multiple intervention sessions. This makes us focus only on the immediate effects of tDCS and ignore the cumulative effects of tDCS on the brain network. Second, there was a lack of clinical data (behavior scores) before and after stimulation of the children with ASD, such as Autism Behavior Checklist (ABC) (Volkmar et al., 1988), Social Communication Questionnaire (SCQ) (Rutter et al., 2007), Social Responsiveness Scale (SRS) (Constantino and Gruber, 2012), and Clancy Behavior Scale (Sun et al., 2013).

In the present study, we were unable to observe improvement of behavior in individuals with ASD due to the absence of clinical data. Nevertheless, it should be emphasized that the aim of the present study was to investigate tDCS modulation of brain functional connectivity. Here we have shown a complex interplay between local and global information processing. In other words, we show that stimulating a focal region can have distal effects on many other brain regions. Despite these general effects, our coarse-level results are merely the first step since much more work must be completed to determine the robustness and credibility of many of these network modulation effects, including longitudinal clinical studies, analyses of correlation with intellectual level, and examining long-lasting effects of stimulation, of which our current study does not tackle.

On the other hand, our results underline the idea that tDCS affects the topological organization of specific functional brain networks at specific frequency bands. This study demonstrates that tDCS can change ongoing network dynamics, some studies have also obtained similar results with Transcranial Magnetic Stimulation (TMS) (Pascual-Leone, 2011). Their results indicate that TMS could lead to cortical plasticity and changes in network dynamics (Pascual-Leone, 2011), which could be a promising approach to the treatment of ASD (Oberman, 2016). A recent study (Lauro, 2014) has focused on the combined effects of TMS and tDCS in the modulation of brain networks. It would be worthwhile for future work to study the similarities and differences in the modulation of brain networks by TMS and tDCS.

## 12. Conclusion

In summary, we applied two network-based methodologies to investigate tDCS-induced network alteration. Our findings highlight the differences in rapid reconfiguration of the resting community organization following tDCS stimulation, and the fundamental modulation in the modular architecture (local and global) of the functional connectivity patterns within specific frequency bands. Our results may help to establish effective tDCS modulation therapy strategies for children with

ASD and other neurological disorders.

### CRedit authorship contribution statement

**Tianyi Zhou:** Writing - original draft, Conceptualization, Methodology, Software. **Jiannan Kang:** Data curation. **Zheng Li:** Writing - review & editing. **He Chen:** Investigation. **Xiaoli Li:** Supervision, Project administration, Funding acquisition.

### Acknowledgements

The authors are extremely thankful to the anonymous reviewers for their helpful suggestions for improving the manuscript. This research was supported by grants from the National Natural Science Foundation of China (grants 61827811 and 61761166003) and the National Key R&D Program of China (grant 2016YFC1306203).

### Appendix A. Supplementary data

Supplementary data to this article can be found online at <https://doi.org/10.1016/j.nicl.2020.102500>.

### References

- Dedoncker, J., Brunoni, A.R., Baeken, C., Vanderhasselt, M.-A., 2016. A Systematic Review and Meta-Analysis of the Effects of Transcranial Direct Current Stimulation (tDCS) Over the Dorsolateral Prefrontal Cortex in Healthy and Neuropsychiatric Samples: Influence of Stimulation Parameters. *Brain Stimulation* 9 (4), 501–517. <https://doi.org/10.1016/j.brs.2016.04.006>.
- Kunze, T., Hunold, A., Haueisen, J., Jirsa, V., Spiegler, A., 2016. Transcranial direct current stimulation changes resting state functional connectivity: a large-scale brain network modeling study. *NeuroImage* 140, 174–187.
- Mancini, M., Brignani, D., Conforto, S., Mauri, P., Miniussi, C., Pellicciari, M.C., 2016. Assessing cortical synchronization during transcranial direct current stimulation: A graph-theoretical analysis. *NeuroImage* 140, 57–65.
- Keiser, D., et al., 2011. Prefrontal transcranial direct current stimulation changes connectivity of resting-state networks during fMRI. *J. Neurosci.* 31 (43), 15284–15293.
- Pellicciari, M.C., Brignani, D., Miniussi, C., 2013. Excitability modulation of the motor system induced by transcranial direct current stimulation: a multimodal approach. *NeuroImage* 83, 569–580.
- Borchers, S., Himmelbach, M., Logothetis, N., Karnath, H.-O., 2012. Direct electrical stimulation of human cortex—the gold standard for mapping brain functions? *Nat. Rev. Neurosci.* 13 (1), 63.
- Keown, C.L., Datko, M.C., Chen, C.P., Maximo, J.O., Jahedi, A., Müller, R.-A., 2017. Network organization is globally atypical in autism: a graph theory study of intrinsic functional connectivity. *Biological Psychiatry: Cognitive Neuroscience and Neuroimaging* 2 (1), 66–75.
- Baio, J., et al., 2018. Prevalence of Autism Spectrum Disorder Among Children Aged 8 Years - Autism and Developmental Disabilities Monitoring Network, 11 Sites, United States, 2014. *MMWR Surveill Summ* 67 (6), 1–23. <https://doi.org/10.15585/mmwr.ss6706a1>.
- Osório, A.A.C., Brunoni, A.R., 2019. Transcranial direct current stimulation in children with autism spectrum disorder: a systematic scoping review. *Dev. Med. Child Neurol.* 61 (3), 298–304.
- Francis, K., 2005. Autism interventions: a critical update. *Dev. Med. Child Neurol.* 47 (7), 493–499.
- MacMaster, F., Sembo, M., Ma, K., Croarkin, P., 2016. Brain stimulation in childhood mental health: Therapeutic applications. *Pediatric Brain Stimulation: Elsevier* 321–344.
- Kang, J., et al., 2018. Transcranial direct current stimulation (tDCS) can modulate EEG complexity of children with autism spectrum disorder. *Frontiers in Neuroscience* 12, 201.
- Van Steenburgh, J.J., Varvaris, M., Schretlen, D.J., Vannorsdall, T.D., Gordon, B., 2017. Balanced bifrontal transcranial direct current stimulation enhances working memory in adults with high-functioning autism: a sham-controlled crossover study. *Molecular Autism* 8 (1), 40.
- Hummel, F., et al., 2005. Effects of non-invasive cortical stimulation on skilled motor function in chronic stroke. *Brain* 128 (3), 490–499.
- Miniussi, C., et al., 2008. Efficacy of repetitive transcranial magnetic stimulation/transcranial direct current stimulation in cognitive neurorehabilitation. *Brain Stimulation* 1 (4), 326–336.
- Bassett, D.S., Wymbs, N.F., Porter, M.A., Mucha, P.J., Carlson, J.M., Grafton, S.T., 2011. Dynamic reconfiguration of human brain networks during learning. *Proc. Natl. Acad. Sci.* 108 (18), 7641–7646.
- Khambhati, A.N., et al., 2015. Dynamic network drivers of seizure generation, propagation and termination in human neocortical epilepsy. *PLoS Comput. Biol.* 11 (12), e1004608.
- Bullmore, E., Sporns, O., 2012. The economy of brain network organization. *Nat. Rev. Neurosci.* 13 (5), 336.
- Bassett, D.S., Brown, J.A., Deshpande, V., Carlson, J.M., Grafton, S.T., 2011. Conserved and variable architecture of human white matter connectivity. *NeuroImage* 54 (2), 1262–1279.
- Zhou, T., Kang, J., Cong, F., Li, X., 2020. Stability-driven non-negative matrix factorization-based approach for extracting dynamic network from resting-state EEG. *Neurocomputing* 389, 123–131. <https://doi.org/10.1016/j.neucom.2020.01.071>.
- Lee, D.D., Seung, H.S., 1999. Learning the parts of objects by non-negative matrix factorization. *Nature* 401 (6755), 788.
- Khambhati, A.N., Mattar, M.G., Wymbs, N.F., Grafton, S.T., Bassett, D.S., 2018. Beyond modularity: Fine-scale mechanisms and rules for brain network reconfiguration. *NeuroImage* 166, 385–399.
- Chai, L.R., et al., 2017. Evolution of brain network dynamics in neurodevelopment. *Network Neurosci.* 1 (1), 14–30.
- Khambhati, A.N., Medaglia, J.D., Karuza, E.A., Thompson-Schill, S.L., Bassett, D.S., 2018. Subgraphs of functional brain networks identify dynamical constraints of cognitive control. *PLoS Comput. Biol.* 14 (7), e1006234.
- Chen, K.-L., Chiang, F.-M., Tseng, M.-H., Fu, C.-P., Hsieh, C.-L., 2011. Responsiveness of the Psychoeducational Profile for children with autism spectrum disorders. *J. Autism Dev. Disord.* 41 (12), 1658–1664.
- Sadler, J.Z., Fulford, B., 2006. Normative warrant in diagnostic criteria: the case of DSM-IV-TR personality disorders. *J. Pers. Disord.* 20 (2), 170–180.
- Poreisz, C., Boros, K., Antal, A., Paulus, W., 2007. Safety aspects of transcranial direct current stimulation concerning healthy subjects and patients. *Brain Res. Bull.* 72 (4–6), 208–214.
- Fertonani, A., Ferrari, C., Miniussi, C., 2015. What do you feel if I apply transcranial electric stimulation? Safety, sensations and secondary induced effects. *Clin. Neurophysiol.* 126 (11), 2181–2188.
- Gandiga, P.C., Hummel, F.C., Cohen, L.G., 2006. Transcranial DC stimulation (tDCS): a tool for double-blind sham-controlled clinical studies in brain stimulation. *Clin. Neurophysiol.* 117 (4), 845–850.
- Lauro, L.J.R., et al., 2014. tDCS increases cortical excitability: Direct evidence from TMS/EEG. *Cortex* 58 (99), e111.
- Ferree, T.C., Luu, P., Russell, G.S., Tucker, D.M., 2001. Scalp electrode impedance, infection risk, and EEG data quality. *Clin. Neurophysiol.* 112 (3), 536–544.
- Rogasch, N.C., et al., 2014. Removing artefacts from TMS-EEG recordings using independent component analysis: importance for assessing prefrontal and motor cortex network properties. *NeuroImage* 101, 425–439.
- Bokil, H., Andrews, P., Kulkarni, J.E., Mehta, S., Mitra, P.P., 2010. Chronux: a platform for analyzing neural signals. *J. Neurosci. Methods* 192 (1), 146–151.
- Kramer, M.A., Eden, U.T., Lepage, K.Q., Kolacznyk, E.D., Bianchi, M.T., Cash, S.S., 2011. Emergence of persistent networks in long-term intracranial EEG recordings. *J. Neurosci.* 31 (44), 15757–15767.
- Mucha, P.J., Richardson, T., Macon, K., Porter, M.A., Onnela, J.-P., 2010. Community structure in time-dependent, multiscale, and multiplex networks. *Science* 328 (5980), 876–878.
- Chai, L.R., Mattar, M.G., Blank, I.A., Fedorenko, E., Bassett, D.S., 2016. Functional Network Dynamics of the Language System. *Cereb. Cortex* 26 (11) p. cercor; bhw238v1.
- Newman, M.E., Girvan, M., 2004. Finding and evaluating community structure in networks. *Phys. Rev. E* 69 (2), 026113.
- Blondel, V.D., Guillaume, J.-L., Lambiotte, R., Lefebvre, E., 2008. Fast unfolding of communities in large networks. *J. Stat. Mech: Theory Exp.* 2008 (10), P10008.
- Bassett, D.S., Wymbs, N.F., Rombach, M.P., Porter, M.A., Mucha, P.J., Grafton, S.T., 2013. Task-based core-periphery organization of human brain dynamics. *PLoS Comput. Biol.* 9 (9), e1003171.
- Kim, J., Park, H., 2011. Fast nonnegative matrix factorization: An active-set-like method and comparisons. *SIAM Journal on Scientific Computing* 33 (6), 3261–3281.
- Kim, J., He, Y., Park, H., 2014. Algorithms for nonnegative matrix and tensor factorizations: a unified view based on block coordinate descent framework. *J. Global Optim.* 58 (2), 285–319.
- Monti, S., Tamayo, P., Mesirov, J., Golub, T., 2003. Consensus clustering: a resampling-based method for class discovery and visualization of gene expression microarray data. *Machine Learning* 52 (1–2), 91–118.
- Greene, D., Cagney, G., Krogan, N., Cunningham, P., 2008. Ensemble non-negative matrix factorization methods for clustering protein-protein interactions. *Bioinformatics* 24 (15), 1722–1728.
- Kuhn, H.W., 1955. The Hungarian method for the assignment problem. *Naval Research Logistics Quarterly* 2 (1–2), 83–97.
- Khambhati, A.N., et al., 2018. Predictive control of electrophysiological network architecture using direct, single-node neurostimulation in humans. *bioRxiv*. <https://doi.org/10.1101/292748>.
- Reckow, J., et al., 2018. Tolerability and blinding of 4x1 high-definition transcranial direct current stimulation (HD-tDCS) at two and three milliamps. *Brain Stimulation* 11 (5), 991–997. <https://doi.org/10.1016/j.brs.2018.04.022>.
- Paneri, B., et al., 2016. Tolerability of Repeated Application of Transcranial Electrical Stimulation with Limited Outputs to Healthy Subjects. *Brain Stimulation* 9 (5), 740–754. <https://doi.org/10.1016/j.brs.2016.05.008>.
- Giordano, J., et al., 2017. Mechanisms and Effects of Transcranial Direct Current Stimulation. *Dose-Response* 15 (1). <https://doi.org/10.1177/1559325816685467>.
- Borckardt, J.J., et al., 2012. A pilot study of the tolerability and effects of high-definition transcranial direct current stimulation (HD-tDCS) on pain perception. *Pain* 13 (2), 112–120. <https://doi.org/10.1016/j.jpain.2011.07.001>.

- Braun, U., et al., 2015. Dynamic reconfiguration of frontal brain networks during executive cognition in humans. *Proc. Natl. Acad. Sci.* 112 (37), 11678–11683.
- Betzel, R.F., Satterthwaite, T.D., Gold, J.I., Bassett, D.S., 2017. Positive affect, surprise, and fatigue are correlates of network flexibility. *Sci. Rep.* 7 (1), 1–10.
- Klein, C., Liem, F., Hänggi, J., Elmer, S., Jäncke, L., 2016. The “silent” imprint of musical training. *Hum. Brain Mapp.* 37 (2), 536–546.
- Palomar-García, M.-Á., Zatorre, R.J., Ventura-Campos, N., Bueichekú, E., Ávila, C., 2017. Modulation of functional connectivity in auditory–motor networks in musicians compared with nonmusicians. *Cereb. Cortex* 27 (5), 2768–2778.
- Li, Q., Wang, X., Wang, S., Xie, Y., Xie, Y., Li, S., 2020. More Flexible Integration of Functional Systems After Musical Training in Young Adults. *IEEE Trans. Neural Syst. Rehabil. Eng.* 28 (4), 817–824. <https://doi.org/10.1109/TNSRE.2020.2977250>.
- Hansen, E.C., Battaglia, D., Spiegler, A., Deco, G., Jirsa, V.K., 2015. Functional connectivity dynamics: modeling the switching behavior of the resting state. *NeuroImage* 105, 525–535.
- Schoffelen, J.-M., Hultén, A., Lam, N., Marquand, A.F., Uddén, J., Hagoort, P., 2017. Frequency-specific directed interactions in the human brain network for language. *Proc. Natl. Acad. Sci.* 114 (30), 8083–8088.
- Vecchio, F., Pellicciari, M.C., Miraglia, F., Brignani, D., Miniussi, C., Rossini, P.M., 2016. Effects of transcranial direct current stimulation on the functional coupling of the sensorimotor cortical network. *NeuroImage* 140, 50–56.
- Notturmo, F., Marzetti, L., Pizzella, V., Uncini, A., Zappasodi, F., 2014. Local and remote effects of transcranial direct current stimulation on the electrical activity of the motor cortical network. *Hum. Brain Mapp.* 35 (5), 2220–2232.
- Spitoni, G.F., Di Russo, F., Cimmino, R.L., Bozzacchi, C., Pizzamiglio, L., 2013. Modulation of spontaneous alpha brain rhythms using low-intensity transcranial direct-current stimulation. *Frontiers in Human Neuroscience* 7, 529.
- Klimesch, W., 1999. EEG alpha and theta oscillations reflect cognitive and memory performance: a review and analysis. *Brain Res. Rev.* 29 (2–3), 169–195.
- Brunel, N., Wang, X.-J., 2003. What determines the frequency of fast network oscillations with irregular neural discharges? I. Synaptic dynamics and excitation-inhibition balance. *J. Neurophysiol.* 90 (1), 415–430.
- Amatachaya, A., et al., 2015. The short-term effects of transcranial direct current stimulation on electroencephalography in children with autism: a randomized crossover controlled trial. *Behav. Neurol.* 2015.
- Mangia, A.L., Pirini, M., Cappello, A., 2014. Transcranial direct current stimulation and power spectral parameters: a tDCS/EEG co-registration study. *Front. Hum. Neurosci.* 8, 601.
- T. Zhou, J. Kang, F. Cong, and D. X. Li, “Early Childhood Developmental Functional Connectivity of Autistic Brains with Non-Negative Matrix Factorization,” *NeuroImage: Clinical*, p. 102251, 2020/03/20/ 2020, doi: <https://doi.org/10.1016/j.nicl.2020.102251>.
- O’Reilly, C., Lewis, J.D., Elsabbagh, M., 2017. Is functional brain connectivity atypical in autism? A systematic review of EEG and MEG studies. *PLoS ONE* 12 (5), e0175870.
- Belmonte, M.K., Allen, G., Beckel-Mitchener, A., Boulanger, L.M., Carper, R.A., Webb, S.J., 2004. Autism and abnormal development of brain connectivity. *J. Neurosci.* 24 (42), 9228–9231.
- Geschwind, D.H., Levitt, P., 2007. Autism spectrum disorders: developmental disconnection syndromes. *Curr. Opin. Neurobiol.* 17 (1), 103–111. <https://doi.org/10.1016/j.conb.2007.01.009>.
- Just, M.A., Cherkassky, V.L., Keller, T.A., Minshew, N.J., 2004. Cortical activation and synchronization during sentence comprehension in high-functioning autism: evidence of underconnectivity. *Brain* 127 (8), 1811–1821.
- Fregni, F., Pascual-Leone, A., 2007. Technology insight: noninvasive brain stimulation in neurology—perspectives on the therapeutic potential of rTMS and tDCS. *Nature Reviews Neurology* 3 (7), 383.
- Lindenberg, R., Renga, V., Zhu, L., Nair, D., Schlaug, G., 2010. Bihemispheric brain stimulation facilitates motor recovery in chronic stroke patients. *Neurology* 75 (24), 2176–2184.
- Floris, D.L., et al., 2016. Atypically rightward cerebral asymmetry in male adults with autism stratifies individuals with and without language delay. *Hum. Brain Mapp.* 37 (1), 230–253.
- Hubl, D., et al., 2003. Functional imbalance of visual pathways indicates alternative face processing strategies in autism. *Neurology* 61 (9), 1232–1237.
- Corbett, B.A., et al., 2009. A functional and structural study of emotion and face processing in children with autism. *Psychiatry Research: Neuroimaging* 173 (3), 196–205.
- Cardinale, R.C., Shih, P., Fishman, I., Ford, L.M., Müller, R.-A., 2013. Pervasive rightward asymmetry shifts of functional networks in autism spectrum disorder. *JAMA Psychiatry* 70 (9), 975–982.
- Amatachaya, A., et al., 2014. Effect of anodal transcranial direct current stimulation on autism: a randomized double-blind crossover trial. *Behav. Neurol.* 2014, 173073. <https://doi.org/10.1155/2014/173073>.
- Volkmar, F.R., Cicchetti, D.V., Dykens, E., Sparrow, S.S., Leckman, J.F., Cohen, D.J., 1988. An evaluation of the autism behavior checklist. *J. Autism Dev. Disord.* 18 (1), 81–97. <https://doi.org/10.1007/BF02211820>.
- M. Rutter, A. Bailey, C. Lord, C. Cianchetti, and G. S. Fancello, *SCQ: Social Communication Questionnaire: Manuale*. Giunti OS, 2007.
- Constantino, J.N., Gruber, C.P., 2012. *Social responsiveness scale: SRS-2*. Western Psychological Services Torrance, CA.
- Sun, X., Allison, C., Auyeung, B., Matthews, F.E., Baron-Cohen, S., Brayne, C., 2013. What is available for case identification in autism research in mainland China? *Research in Autism Spectrum Disorders* 7 (5), 579–590.
- Pascual-Leone, A., et al., 2011. Characterizing brain cortical plasticity and network dynamics across the age-span in health and disease with TMS-EEG and TMS-fMRI. *Brain Topogr.* 24 (3–4), 302.
- Oberman, L.M., et al., 2016. Transcranial magnetic stimulation in autism spectrum disorder: challenges, promise, and roadmap for future research. *Autism Research* 9 (2), 184–203.